ISSN 1392-1207. MECHANIKA. Vol. 30, No. 5, 2024: 423–429

Performance of a Small Hydrodynamic Journal Bearing Involving Adsorbed Layer and Surface Elastic Deformation

Shuxiong XIAO, Yongbin ZHANG
College of Mechanical Engineering, Changzhou University, Changzhou, Jiangsu Province, China,
E-mails: yongbinzhang@cczu.edu.cn, engmech1@sina.com (Corresponding author)

https://doi.org/10.5755/j02.mech.37032

1. Introduction

The small hydrodynamic journal bearing with the diameter of the rotating shaft on the 1mm scale or less has its specifically important application in industry or ordinary life such as in medical apparatus, small equipments and micro machines etc. The working principle and design method of this bearing are actually different from those of the classical journal bearing [1] as it involves more complicated hydrodynamic phenomena. One factor is the effect of the physically adsorbed layer intrinsically present on the bearing surface which may be significant, as the bearing clearance can be so small. Another factor is the continuum hydrodynamic fluid film which may still be existent in the bearing. These two factors thus result in the multiscale flow in the bearing [2, 3]. The adsorbed layer flow is molecular-scale, while the continuum fluid flow is macroscopic. New hydrodynamic theories thus need to be developed for this small-size bearing, rather than using classical hydrodynamic theories [1].

Owing to the interaction between the fluid and the bearing surface, the adsorbed layer is packed, and its rheological properties like the density and viscosity are different from its bulk values [4, 5]. There is also the non-continuum effect in such a layer. Classical multiscale schemes use molecular dynamics simulation to model the adsorbed layer flow while use the continuum fluid model to simulate the continuum fluid flow [6-8]. As a journal bearing possesses the engineering sizes, these multiscale schemes are presently actually incapable to simulate the multiscale flow in the above mentioned small bearing because of too high computational cost.

In recent years, Zhang derived the closed-form explicit mathematical equations respectively for the adsorbed layer flow and the intermediate continuum fluid flow in the two-dimensional multiscale flow problem [9].

In the former studies, Gu and Zhang analytically studied the load performance of the hydrodynamic journal bearing with conventional sizes (on the 10mm scale) with the eccentricity ratios subjected to approaching to unity, where the flow is indeed multiscale because of the locally very low bearing clearances [10]. They assumed the bearing surfaces as elastic and showed the very significant effect of the adsorbed layer on the load-carrying capacity of the bearing.

Specifically, the present paper studies the load and friction performances of the small hydrodynamic journal bearing with the radius of the rotating shaft equal to 1 mm for the widely varying eccentricity ratios from 0.1 to nearly unity, by using Zhang's multiscale flow equations. The bearing surfaces are considered as elastic and the calculation results are compared with those for rigid surfaces. The results of the frictional coefficient of this bearing are also calculated based on the multiscale flow theory. The obtained load and friction results of this small bearing are largely different from the classical recognition, showing the important influence of the adsorbed layer. They should be of significance to the design and application of the mentioned type of the bearing.

2. The Small Elastohydrodynamic Journal Bearing

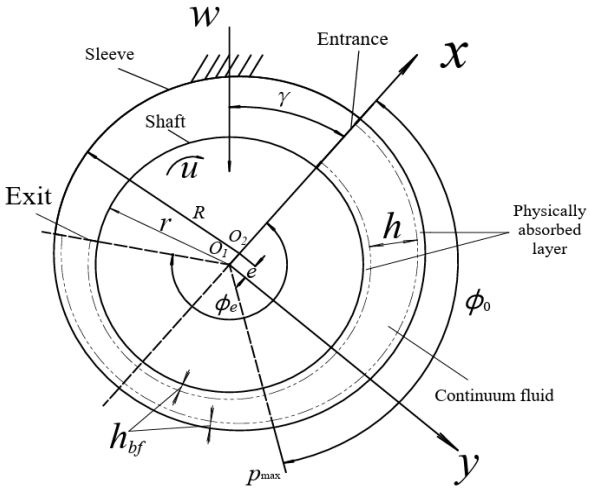

Fig. 1 The magnified picture of the studied small hydrodynamic journal bearing involving the adsorbed layer and the surface elastic deformation

Fig. 1 describes the configuration of the small elastohydrodynamic journal bearing the diameter of which may be on the scales of 0.1-1.0 mm or less. These small journal bearings have specific applications in micro apparatus or micro machines to support the load. Because of their downsizing, their sliding speeds may be low and their characteristic feature is the very low bearing clearances even for the normal eccentricity ratio, which is on the scale of 0.1. The thickness of the physically adsorbed layer on the bearing surface thus becomes comparable to the intermediate continuum fluid film thickness. The adsorbed layer effect should consequently be strongly involved. The notations are: e – eccentricity, h_{bf} – adsorbed layer thickness, h – continuum fluid film thickness, p_{max} – maximum film pressure, r – shaft radius, R – sleeve radius, u – circumferential velocity, ϕ_0 – angular coordinate of the maximum film pressure position, ϕ_e – angular coordinate of the exit of the bearing. The used x and y coordinates are shown in Fig. 1.

3. Mathematical Analysis

Here, the analysis is based on Zhang's multiscale flow equations [9]. It assumes that:
a. The fluid is Newtonian;
b. There is no interfacial slippage;
c. No side leakage occurs;
d. The two adsorbed layers are identical;
e. The bearing surfaces are ideally smooth;
f. The condition is isothermal and steady-state.

For the used low sliding speed, assumptions a, b and f are valid. For the same shaft and sleeve surface materials, assumption d is valid. For the ratio of the bearing axial length to the shaft diameter over 8, assumption c is valid; Regarding the effect of the bearing surface roughness which may be on the molecular scale, the work will be done further.

3.1. Fundamental equations for mass continuity, film pressure and load

The total mass flow rate per unit contact length through the bearing is [9, 10]:

$$q_m = uh_{bf}\rho_{bf}^{eff} + \frac{uh}{2}\rho + \left(\frac{h_{bf}^3 G_1 + h^3 G_2}{r}\cdot\frac{\partial p}{\partial \phi}\right), \tag{1}$$

where $c = R - r$, ϕ is the angular coordinate, ρ_{bf}^{eff} and η_{bf}^{eff} are respectively the average density and the effective viscosity of the adsorbed layer, ρ is the fluid bulk density, p is the hydrodynamic pressure, G_1 and G_2 are respectively:

$$G_1 = \frac{\rho_{bf}^{eff}}{\eta_{bf}^{eff}}\left[\frac{F_1}{6} - \frac{\varepsilon_0}{1+\frac{\Delta x}{D}}\left(1 + \frac{1}{2\lambda_{bf}} - \frac{q_0 - {q_0}^n}{{q_0}^{n-1} - {q_0}^n}\frac{\Delta_{n-2}}{h_{bf}}\right)\right], \tag{2}$$

$$G_2 = \frac{\rho}{\eta_{bf}^{eff}}\left[\frac{F_2\lambda_{bf}^2}{6} - \frac{\lambda_{bf}}{1+\frac{\Delta x}{D}}\left(\frac{1}{2} + \lambda_{bf} - \frac{q_0 - {q_0}^n}{{q_0}^{n-1} - {q_0}^n}\frac{\Delta_{n-2}}{h_{bf}}\right) - \frac{\eta_{bf}^{eff}}{12\eta}\right]. \tag{3}$$

In Eqs. (2) and (3), $\lambda_{bf} = h_{bf}/h$, D is the fluid molecule diameter, η is the fluid bulk viscosity, Δx is the circumferential separation of the neighboring fluid molecules in the adsorbed layer, n the equivalent number of the fluid molecules across the adsorbed layer thickness, q_0 (>1) is the average value of Δ_{j+1}/Δ_j (Δ_j is the separation between the $(j+1)^{\text{th}}$ and j^{th} fluid molecules across the adsorbed layer thickness), Δ_{n-2} is the separation between the neighboring fluid molecules across the adsorbed layer thickness just on the adsorbed layer-fluid interface, and ε, F_1 and F_2 are the parameters reflecting the non-continuum effect of the adsorbed layer and their formulations have been shown in [9].

There are the (N+1) discretized points in the initially set simulated lubricated area. By considering the elastic deformations of the bearing surfaces, the continuum fluid film thickness on the i^{th} discretized point is:

$$h_i = c + e\cos\phi_i - 2h_{bf} - \frac{2r}{\pi E_v}\int_0^{\phi_e} p(\phi_s)\ln\left(r\phi_i - r\phi_s\right)^2 d\phi_s,$$

for i = 1, 2, …, N (exit), (4)

where e is the bearing eccentricity as shown in Fig. 1, and E_v is the equivalent Young's modulus of elasticity of two bearing surfaces.

By forward difference of Eq. (1) and using the boundary condition $p_0 = 0$, it is finally expressed that [10]:

$$p_i = r\cdot\Delta\phi\sum_{j=1}^{i}\frac{q_m - \frac{u\rho h_i}{2} - uh_{bf}\rho_{bf}^{eff}}{h_i^3 G_2 + h_{bf}^3 G_1},$$

for i = 1, 2, ..., N. (5)

The film force per unit contact length acting in the x coordinate direction is:

$$w_x = \Delta\phi\sum_{i=1}^{N} p_i\cos\phi_i = r(\Delta\phi)^2\sum_{i=1}^{N}\left[\cos\phi_i\cdot\sum_{j=1}^{i}\frac{q_m - \frac{u\rho h_i}{2} - uh_{bf}\rho_{bf}^{eff}}{h_i^3 G_2 + h_{bf}^3 G_1}\right]. \tag{6}$$

The film force per unit contact length acting in the y coordinate direction is:

$$w_y = \Delta\phi\sum_{i=1}^{N} p_i\sin\phi_i = r(\Delta\phi)^2\sum_{i=1}^{N}\left[\sin\phi_i\cdot\sum_{j=1}^{i}\frac{q_m - \frac{u\rho h_i}{2} - uh_{bf}\rho_{bf}^{eff}}{h_i^3 G_2 + h_{bf}^3 G}\right]. \tag{7}$$

The load per unit contact length of the bearing is:

$$w = \sqrt{{w_x}^2 + {w_y}^2}. \tag{8}$$

3.2. Shear stress and friction coefficient

The shear stress on the sleeve surface is [9]:

$$\tau_h = \frac{v_A - \bar{u}_a - \frac{\partial p}{\partial x}D\sum_{j=1}^{n-1}\frac{j\Delta_{j-1}}{\eta_{line,j-1}}}{\sum_{j=1}^{n-1}\frac{\Delta_{j-1}}{\eta_{line,j-1}}} + \frac{\partial p}{\partial x}D, \tag{9}$$

where $\eta_{line,\,j\text{-}1}$ is the local viscosity between the j^{th} and $(j-1)^{th}$ fluid molecules across the adsorbed layer thickness, v_A is the boundary velocity of the continuum film adjacent to the sleeve surface, and $\bar{u}_a$ is the fluid molecule velocity on the sleeve surface and here $\bar{u}_a = 0$.

The shear stress on the shaft surface is [9]:

$$\tau_s = -\frac{v_B - \bar{u}_b - \dfrac{\partial p}{\partial x} D \sum_{j=1}^{n-1} \dfrac{j\Delta_{j-1}}{\eta_{line\,,j-1}}}{\sum_{j=1}^{n-1} \dfrac{\Delta_{j-1}}{\eta_{line\,,j-1}}} - \frac{\partial p}{\partial x} D\,, \tag{10}$$

where v_B is the boundary velocity of the continuum film adjacent to the shaft surface, and $\bar{u}_b$ is the fluid molecule velocity on the shaft surface and here $\bar{u}_b = u$.

It is formulated that [9]:

$$v_A = \bar{u}_a + \frac{\partial p}{\partial x} D \sum_{j=1}^{n-1} \frac{j\Delta_{j-1}}{\eta_{line\,,j-1}} + \frac{(\bar{u}_b - \bar{u}_a)\eta}{2\eta \sum_{j=1}^{n-1} \dfrac{\Delta_{j-1}}{\eta_{line\,,j-1}} + h} \sum_{j=1}^{n-1} \frac{\Delta_{j-1}}{\eta_{line\,,j-1}} - \frac{\partial p}{\partial x}\left(\frac{h}{2} + Dn\right) \sum_{j=1}^{n-1} \frac{\Delta_{j-1}}{\eta_{line\,,j-1}}\,, \tag{11}$$

$$v_B = \bar{u}_a + \frac{\partial p}{\partial x} D \sum_{j=1}^{n-1} \frac{j\Delta_{j-1}}{\eta_{\text{line}\,,j-1}} + \frac{\bar{u}_b - \bar{u}_a}{\dfrac{2\eta}{h} \sum_{j=1}^{n-1} \dfrac{\Delta_{j-1}}{\eta_{\text{line}\,,j-1}} + 1} \left(\frac{\eta}{h} \sum_{j=1}^{n-1} \frac{\Delta_{j-1}}{\eta_{\text{line}\,,j-1}} + 1 \right) - \frac{\partial p}{\partial x}\left(\frac{h}{2} + Dn\right) \sum_{j=1}^{n-1} \frac{\Delta_{j-1}}{\eta_{\text{line}\,,j-1}}\,. \tag{12}$$

Assume that $\eta_{line,j} / \eta_{line,j+1} = q^{\gamma}_0$, where γ is constant [9]. It is obtained that:

$$\sum_{j=1}^{i} \frac{\Delta_{j-1}}{\eta_{line\,,j-1}} = \frac{\Delta_{n-2}\left[q_0^{(1+\gamma)(i-n+2)} - q_0^{-(n-2)(1+\gamma)}\right]}{\eta_{line,n-2}\left[q_0^{(1+\gamma)} - 1\right]}, \quad \text{for } i = 1, 2, \ldots, (n\text{-}1), \tag{13}$$

$$\sum_{j=1}^{i} \frac{j\Delta_{j-1}}{\eta_{line\,,j-1}} = \frac{\Delta_{n-2}}{\eta_{line,n-2}} \left[\frac{q_0^{(2-n)(1+\gamma)} - q_0^{(1+\gamma)(i-n+2)}}{(q_0^{1+\gamma} - 1)^2} + \frac{i q_0^{(1+\gamma)(i-n+2)}}{q_0^{1+\gamma} - 1} \right] \quad \text{for } i = 1, 2, \ldots, (n\text{-}1). \tag{14}$$

Substituting Eqs. (11), (13) and (14) into Eq. (9) gives that:

$$\tau_h = \frac{\eta(\bar{u}_b - \bar{u}_a)}{\dfrac{2\Delta_{n-2}\left[q_0^{(1+\gamma)} - q_0^{-(n-2)(1+\gamma)}\right]}{q_0^{1+\gamma} - 1} + h} - \frac{\partial p}{\partial x}\left(\frac{h}{2} + D(n-1)\right). \tag{15}$$

Substituting Eqs. (12), (13) and (14) into Eq. (10) gives that:

$$\tau_s = \frac{\eta(\bar{u}_b - \bar{u}_a)}{\dfrac{2\Delta_{n-2}\left[q_0^{(1+\gamma)} - q_0^{-(n-2)(1+\gamma)}\right]}{q_0^{1+\gamma} - 1} + h} + \frac{\partial p}{\partial x}\left(\frac{h}{2} + D(n-1)\right). \tag{16}$$

The friction forces per unit contact length on the sleeve and shaft surfaces are respectively:

$$F_h = r \sum_{i=1}^{N} \tau_{h,i} \cdot \Delta\phi\,, \tag{17}$$

$$F_s = r \sum_{i=1}^{N} \tau_{s,i} \cdot \Delta\phi\,. \tag{18}$$

The friction coefficients on the sleeve and shaft surfaces are respectively:

$$f_h = \frac{|F_h|}{w} \quad \text{and} \quad f_s = \frac{|F_s|}{w}. \tag{19}$$

3.3. Numerical calculation of the surface elastic deformation, numerical solution procedure and formulation of the operational parameters

The numerical calculation of the surface elastic deformation and the numerical solution procedure can be found from [10]. Through the numerical procedure, the Reynolds boundary condition [1] is satisfied on the exit of the bearing. We developed the computing software by ourselves through the MATLAB platform. The dependence of the fluid viscosity and density on the fluid pressure was considered. Their formulations were shown in [11]. The weak, medium and strong fluid-bearing surface interactions were respectively considered. The values of the parameters for characterizing them were also mentioned in [11].

4. Calculation Results

In all the calculations, the following operational parameter values have been used [10]:
$\Delta x/D = \Delta_{n\text{-}2}/D = 0.15$, $d = 0.5$ nm, $r = 1$ mm, c = 0.1 μm, $\zeta = 1.6\times10^{-8}$ m^2/N, $\eta_a = 0.03$ Pa·s, $\beta = 0.4\times10^{-9}$ Pa^{-1}, $E_v = 2.09\times10^{11}$ Pa, $N = 2500$.

The values of u and ε are chosen such that the generated maximum film pressures in the bearing are mostly on the scale of 1 MPa and give the practical loads within the scope of the mechanical strength of a micro apparatus.

4.1. Film pressure distribution

Fig. 2, a shows the film pressure distributions in the bearing for different contact regimes and different fluid-bearing surface interactions when $u = 10$ μm/s and $\varepsilon = 0.9$. For elastic surfaces, the effect of the fluid-bearing surfaces interaction on the film pressure is weaker than that for rigid surfaces. However, whenever the bearing surfaces are rigid or elastic, the effect of the adsorbed layer very significantly increases the load-carrying capacity of the bearing for the medium or strong fluid-bearing surface interactions. For this very low sliding speed, for the weak interaction, the pressure distribution in the elastic contact is nearly overlaid with those in the rigid contact or calculated from the classical hydrodynamic lubrication theory [1]. For a given operating condition, the pressure in the elastic contact is much lower than that in the rigid contact for the medium or strong interactions even for such a low speed.

Fig. 2, b shows that when the sliding speed is increased to 1 mm/s, for $\varepsilon = 0.2$ this phenomenon popularly exists for whichever interaction; It indicates the overall significant effect of the surface elastic deformation in the given operating condition. For the elastic contact, the pressures are even lower than those calculated from the classical hydrodynamic lubrication theory if the interaction is medium or weak. Fig. 2, c shows that in the elastic contact the effect of the sliding speed on the film pressure is weaker than that in the rigid contact, as an example for $\varepsilon = 0.2$ and the strong fluid-bearing surface interaction.

4.2. Bearing load

Fig. 3, a shows that when $u = 10$ μm/s, for $\varepsilon \le 0.8$, the influence of the surface elastic deformation on the carried load of the bearing is negligible for the given three fluid-bearing surface interactions; It should be due to the generated low pressures. However, for $\varepsilon \ge 0.9$ the carried loads of the elastic contact are considerably smaller than those of the rigid contact for the three interactions. This should be due to the generated higher pressures which cause pronounced surface elastic deformations.

Fig. 3, b shows that when $u = 0.1$ mm/s, the influence of the surface elastic deformation on the bearing load is stronger than in Fig. 3, a. In this case, for elastic surfaces the effect of the fluid-surface interaction on the carried load is much reduced as compared to Fig. 3, a.

4.3. Minimum bearing clearance

Fig. 4, a shows that when $u = 10$ μm/s, for $\varepsilon \le 0.8$, the effect of the fluid-surface interaction on the minimum bearing clearance ($h_{tot,min}$) is negligible. In these conditions, although the surface elastic deformation

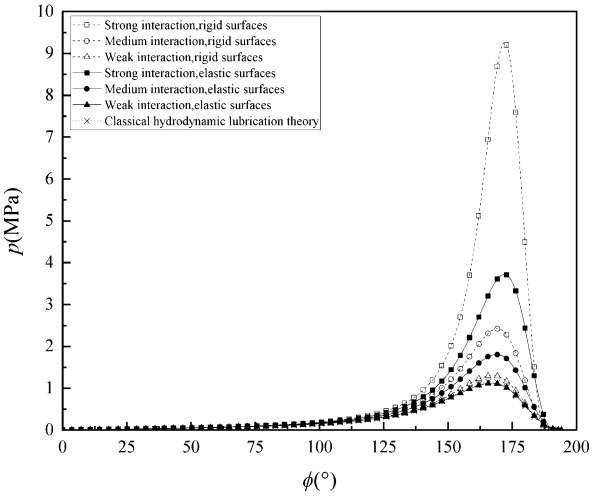

a

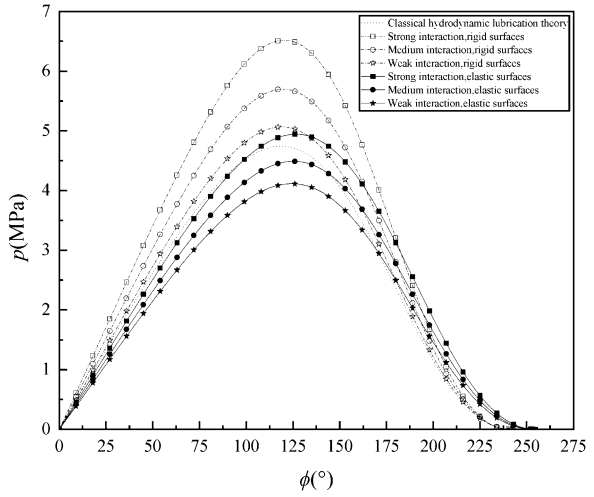

b

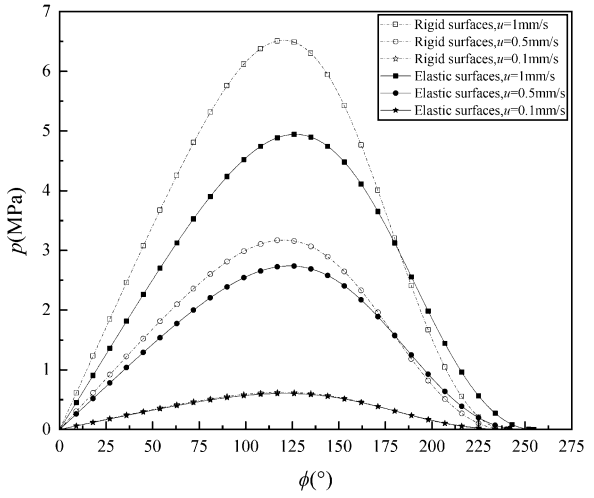

c

Fig. 2 Film pressure distributions in the bearing for different cases: a – $u = 10$ μm/s, $\varepsilon = 0.9$, b – $u = 1$ mm/s, $\varepsilon = 0.2$, c – for $\varepsilon = 0.2$ and the strong fluid-bearing surface

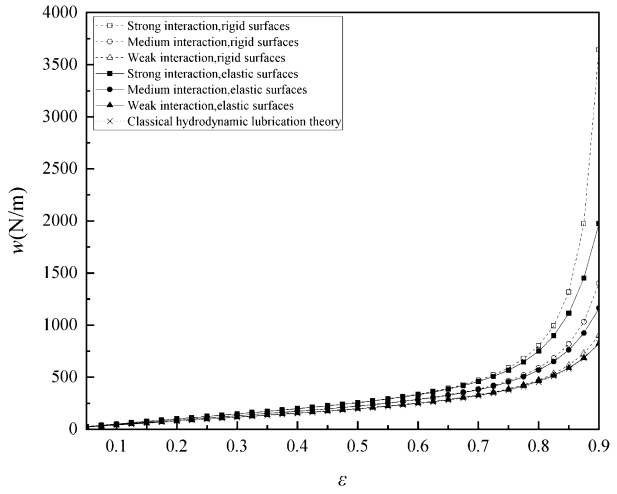

a

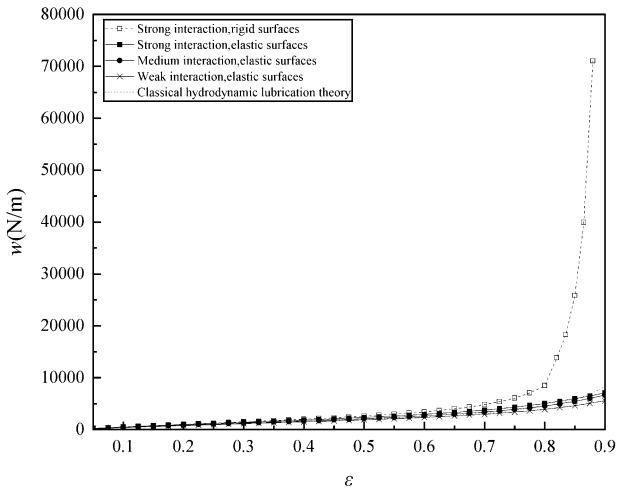

b

Fig. 3 The carried loads of the bearing for different conditions: a – u = 10 μm/s, b – u = 0.1 mm/s

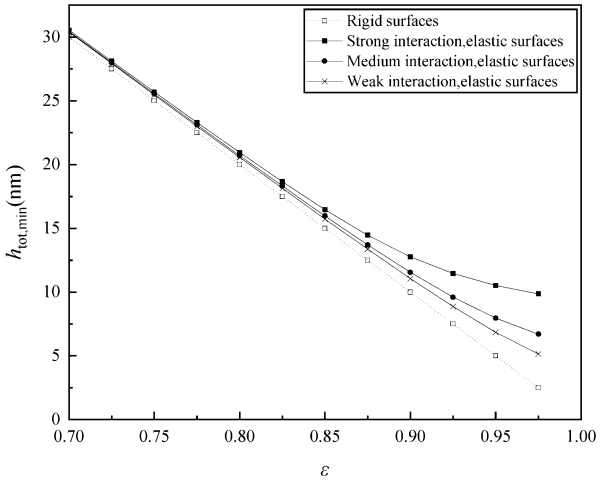

a

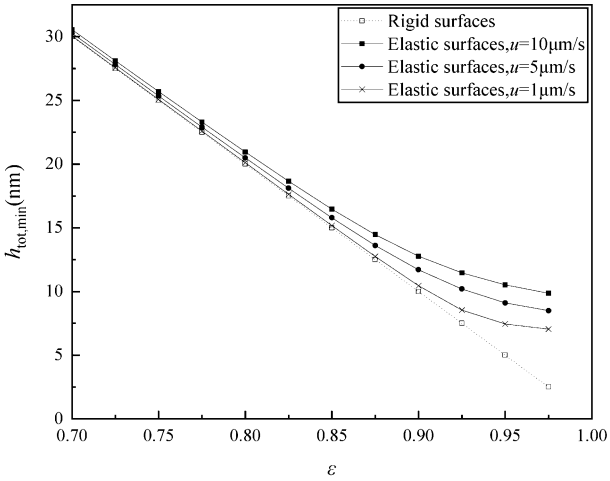

b

Fig. 4 Minimum bearing clearances for different operating conditions: a – u = 10 μm/s, b – for the strong fluid-surface interaction

result in the higher values of $h_{tot,min}$, the influence of the surface elastic deformation on the minimum bearing clearance is quite weak. However, for $\varepsilon \geq 0.9$ both the stronger fluid-surface interaction and the surface elastic deformation result in considerably higher values of $h_{tot,min}$. For the strong interaction, the minimum bearing clearance for the elastic contact is much higher than that for the rigid contact.

Fig. 4, b shows the influence of the sliding speed on the minimum bearing clearance when the bearing surfaces are elastic and the fluid-surface interaction is strong. For $\varepsilon \leq 0.8$, this influence is weak. However, for $\varepsilon \geq 0.9$ this influence is very significant, and the speed increase effectively enlarges the minimum bearing clearance. Even for ε approaching to unity and for the very low sliding speed 1 μm/s, a residual film appears to exist, giving the values of $h_{tot,min}$ more than 5 nm. This result is radically different from the conventional recognition (for rigid surfaces).

4.4. Shear stress and friction coefficient on the bearing surface

Fig. 5, a and b respectively show the shear stress distributions on the shaft and sleeve surfaces when ε = 0.9 and u = 1000 μm/s. For the same fluid-surface interaction, the magnitudes of the shear stresses on both the bearing surfaces for the elastic contact regime are overall smaller than those for the rigid contact regime. When the fluid-surface interaction is stronger, the magnitudes of the shear stresses on both the bearing surfaces are greater. However, the surface elastic deformation much reduces the sensitivity of the surface shear stress to the fluid-surface interaction.

Figs. 6, a-b show that the friction coefficients on the bearing surfaces calculated from the present model are significantly smaller than those calculated from classical hydrodynamic lubrication theory especially for small eccentricity ratios whenever the bearing surfaces are elastic or rigid and the fluid-surface interaction is weak, medium or strong. The surface elastic deformation results in the higher friction coefficient especially for large eccentricity ratios and the strong fluid-surface interaction as compared to the results for rigid surfaces. For a given eccentricity ratio, if the fluid-surface interaction is stronger, the friction coefficient on the bearing surface is smaller. This is particularly the

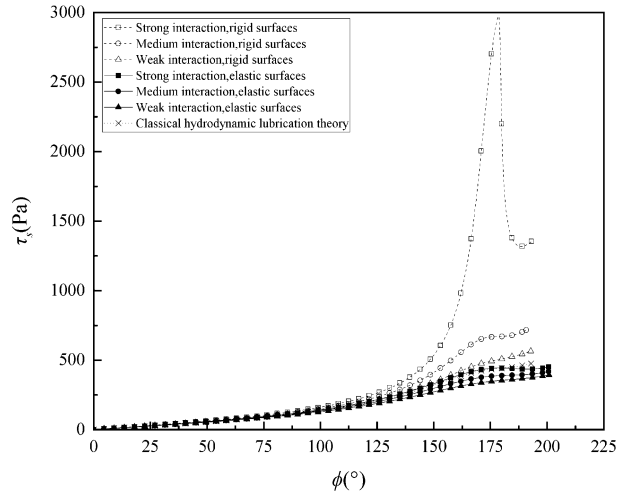

a

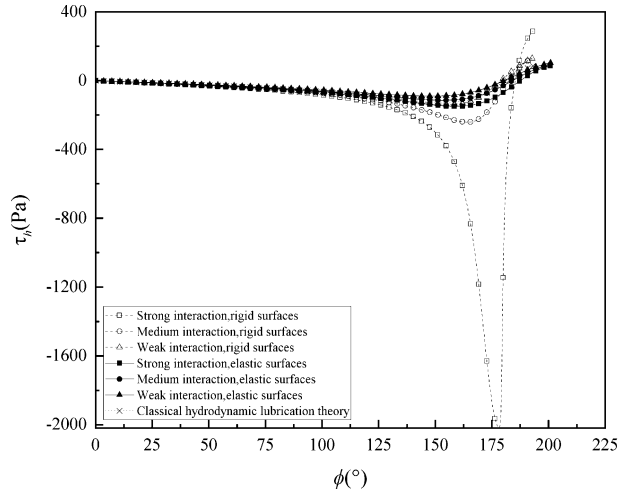

b

Fig. 5 Shear stress distributions respectively on the shaft and sleeve surfaces when $\varepsilon = 0.9$ and $u = 1000$ μm/s: a – shear stress on the shaft surface, b – shear stress on the sleeve surface

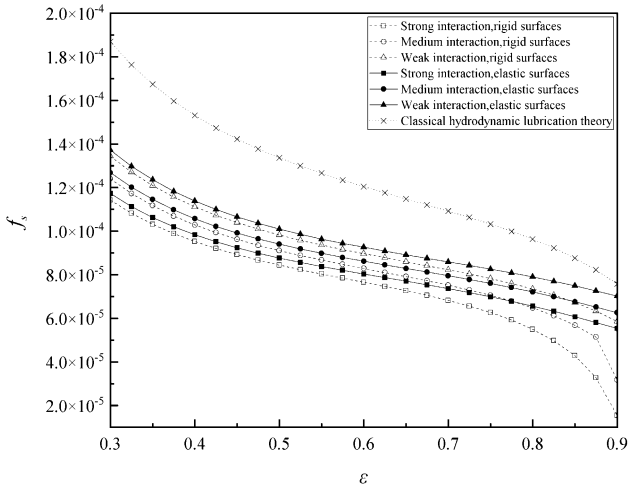

a

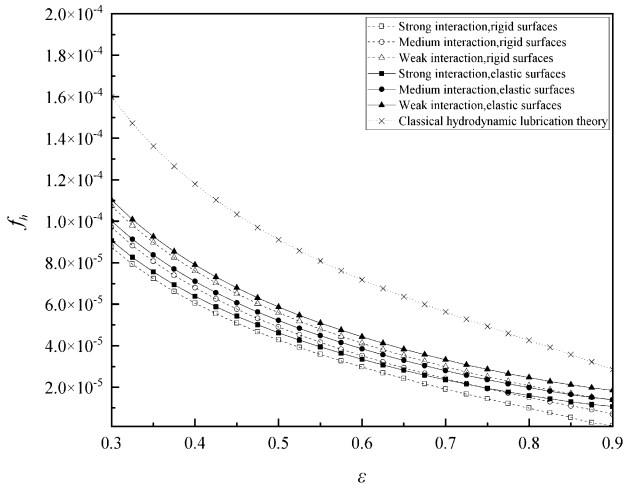

b

Fig. 6 Friction coefficients respectively on the shaft and sleeve surfaces when $\varepsilon = 0.9$ and $u = 1000$ μm/s: a – friction coefficient on the shaft surface, b – friction coefficient on the sleeve surface

case for rigid surfaces and large eccentricity ratios.

5. Conclusions

The load and friction performances of a small hydrodynamic lubricated journal bearing with the shaft radius equal to 1mm are analytically investigated by using the multiscale hydrodynamic flow model. Both the adsorbed layer on the bearing surface and the continuum hydrodynamic fluid contribute to the bearing performance. The molecular-scale non-continuum adsorbed layer flow becomes comparable to the flow of the intermediate continuum fluid film. The hydrodynamic flow in this bearing is thus essentially multiscale. The rigid and elastic bearing surfaces are respectively considered. The fluid-bearing surface interaction is respectively considered as weak, medium and strong. Zhang's multiscale flow equations [9] are used for fast solving the film pressure, carried load and friction coefficient of the bearing.

According to the calculations results, the conclusions are drawn as follows:

a. The effect of the surface elastic deformation is overall significant in the bearing. It results in the reductions of the film pressure and carried load of the bearing for a given eccentricity ratio especially for large eccentricity ratios and the strong fluid-bearing surface interaction;

b. In the elastic contact the effect of the sliding speed on the film pressure is weaker than that in the rigid contact;

c. For large eccentricity ratios such as $\varepsilon \geq 0.9$, both the strong fluid-surface interaction and the surface elastic deformation result in the considerably higher value of the minimum bearing clearance than the classical hydrodynamic theory gives (for rigid surfaces and ignoring the fluid-surface interaction);

d. For large eccentricity ratios such as $\varepsilon \geq 0.9$, when the bearing surfaces are elastic and the fluid-surface interaction is strong, the increase of the sliding speed effectively enlarges the minimum bearing clearance. Even for the eccentricity ratio ε approaching to unity and for the very low sliding speed 1μm/s, a residual film was found to exist, giving the minimum bearing clearance more than 5 nm;

e. For a given fluid-surface interaction, the magnitudes of the shear stresses on the elastic bearing surfaces are overall smaller than those on the rigid bearing surfaces; The magnitudes of the shear stresses on both the bearing surfaces are increased with the increase of the interaction strength between the fluid and the bearing surface. The surface elastic deformation results in the reduced sensitivity of the surface shear stress to the fluid-surface interaction;

f. The friction coefficient of the bearing calculated from the present model is significantly smaller than that calculated from classical hydrodynamic lubrication theory especially for small eccentricity ratios. The surface elastic deformation results in the higher friction coefficient especially for large eccentricity ratios and the strong fluid-surface interaction as compared to the results for rigid surfaces. However, a stronger fluid-surface interaction gives a smaller friction coefficient of the bearing especially for rigid surfaces and large eccentricity ratios.

References

1. **Pinkus, O.; Sternlicht, B.** 1961. Theory of hydrodynamic lubrication. New York: McGraw-Hill. 465p.
2. **O'Connell, S. T.; Thompson, P. A.** 1995. Molecular dynamics–continuum hybrid computations: A tool for studying complex fluid flows, Physical Review E 52: R5792-R5795. https://doi.org/10.1103/PhysRevE.52.R5792.
3. **Aktas, O.; Aluru, N. R.** 2002. A combined continuum/DSMC technique for multiscale analysis of microfluidic filters, Journal of Computational Physics 178(2): 342-372. https://doi.org/10.1006/jcph.2002.7030.
4. **Brown, C. E.; Everett, D. H.; Powell, A. V. Thorne, P. E.** 1975. Adsorption and structuring phenomena at the solid/liquid interface, Faraday Discussion of the Chemical Society 59: 97-108. https://doi.org/10.1039/dc9755900097.
5. **Grosse-Rhode, M.; Findenegg, G. H.** 1978. Formation of ordered monolayers of *n*-alkanes at the cleavage face of nickel chloride, Journal of Colloid and Interface Science 64(2): 374-376. https://doi.org/10.1016/0021-9797(78)90375-2.
6. **Yen, T. H.; Soong, C. Y.; Tzeng, P. Y.** 2007. Hybrid molecular dynamics-continuum simulation for nano/mesoscale channel flows, Microfluidics and Nanofluidics 3: 665-675. https://doi.org/10.1007/s10404-007-0154-7.
7. **Liu, J.; Chen, S.; Nie, X.; Robbins, M. O.** 2007. Continuum-atomistic simulation of heat transfer in micro- and nano-flows, Journal of Computational Physics 227(1): 279-291. https://doi.org/10.1016/j.jcp.2007.07.014.
8. **Nie, X. B.; Chen, S.; Robbins, M. O.** 2004. A continuum and molecular dynamics hybrid method for micro- and nano- fluid flow, Journal of Fluid Mechanics 500: 55-64. https://doi.org/10.1017/S0022112003007225.
9. **Zhang, Y. B.** 2020. Modeling of flow in a very small surface separation, Applied Mathematical Modelling 82: 573-586. https://doi.org/10.1016/j.apm.2020.01.069.
10. **Gu, K. C.** 2024. Study on multiscale lubrication mechanism of journal bearing by considering surface physically adsorbed layer effect, MSc thesis, Changzhou University (in Chinese).
11. **Wang, C.; Zhang, Y. B.** 2004. Multiscale elastohydrodynamic wedge-platform thrust bearing with ultra low clearance, Mechanika 30(1): 23-28. https://doi.org/10.5755/j02.mech.34137.

S. Xiao, Y. Zhang

PERFORMANCE OF A SMALL HYDRODYNAMIC JOURNAL BEARING INVOLVING ADSORBED LAYER AND SURFACE ELASTIC DEFORMATION

S u m m a r y

The load and friction performances of a small elastohydrodynamic journal bearing with the shaft radius 1mm have been computationally studied. The effect of the adsorbed layer is incorporated and the multiscale hydrodynamic flow theory is used. It is shown that the multiscale performance of this bearing occurs in the wide eccentricity ratio range from 0.3 to nearly unity because of the influence of the adsorbed layer, and thus the generated pressures and carried load of this bearing are significantly greater than the classical hydrodynamic theory calculations. The effect of the adsorbed layer is more stronger for rigid bearing surfaces than for elastic bearing surfaces especially for a strong fluid-bearing surface interaction, and it is strong for the high eccentricity ratios over 0.9. In this bearing, when the effect of the adsorbed layer is incorporated, the friction coefficients on both bearing surfaces are reduced in the wide eccentricity ratio range as compared to the classical calculation; Stronger the fluid-bearing surface interaction, greater the reduction of the friction coefficient, showing the pronounced non-continuum effect of the adsorbed layer. However, for elastic surfaces the friction coefficient is a bit higher than that for rigid surfaces especially for high eccentricity ratios and strong fluid-bearing surface interactions.

Keywords: adsorbed layer, elastohydrodynamics, journal bearing, multiscale.

Received April 22, 2024
Accepted October 22, 2024